Research Article Vol. 60, No. 35 / 10 December 2021 / Applied Optics 10975

applied optics

Numerical investigations into polarization-induced self-powered GaN-based MSM photodetectors

Jiaxing Wang,[1,2] Chunshuang Chu,[1,2,4] Jiamang Che,[1,2] Hua Shao,[1,2] Yonghui Zhang,[1,2] Xiaojuan Sun,[3] Zi-Hui Zhang,[1,2,*] and Dabing Li[3]

[1]State Key Laboratory of Reliability and Intelligence of Electrical Equipment, Hebei University of Technology, Tianjin 300401, China
[2]Key Laboratory of Electronic Materials and Devices of Tianjin, School of Electronics and Information Engineering, Hebei University of Technology, Tianjin 300401, China
[3]State Key Laboratory of Luminescence and Applications, Changchun Institute of Optics, Fine Mechanics and Physics, Chinese Academy of Sciences, Changchun 130033, China
[4]e-mail: chuchunshuang@hotmail.com
*Corresponding author: zh.zhang@hebut.edu.cn

Received 4 October 2021; revised 15 November 2021; accepted 15 November 2021; posted 16 November 2021; published 8 December 2021

Traditional GaN-based metal-semiconductor-metal (MSM) photodetector (PD) features a symmetric structure, and thus a poor lateral carrier transport can be encountered, which can decrease the photocurrent and responsivity. To improve its photoelectric performance, we propose GaN-based MSM photodetectors with an AlGaN polarization layer structure on the GaN absorption layer. By using the AlGaN polarization layer, the electric field in the metal/GaN Schottky junction can be replaced by the electric fields in the metal/AlGaN Schottky junction and the AlGaN/GaN heterojunction. The increased polarization electric field can enhance the transport for the photogenerated carriers. More importantly, such polarization electric field cannot be easily screened by free carriers, thus showing the detectability for the even stronger illumination intensity. Moreover, we also conduct in-depth parametric investigations into the impact of different designs on the photocurrent and the responsivity. Hence, device physics regarding such proposed MSM PDs has been summarized. © 2021 Optica Publishing Group

https://doi.org/10.1364/AO.445069

1. INTRODUCTION

Because of the advantages of wide direct bandgap, high electron saturation velocity, high thermal conductivity, and excellent chemical and physical stability [1], GaN and its ternary compound materials have been widely applied in light-emitting diodes (LEDs), power devices, photodetectors (PDs) and so on [2–4]. Among the GaN-based semiconductor devices, GaN-based PDs have attracted enormous interest in environmental monitoring, missile detection, flame detection, UV communications and so on [5,6]. Since the first photoconductive ultraviolet detector based on insulating single-crystal GaN was successfully fabricated by Khan *et al*. in 1992 [7], GaN-based PDs have undergone rapid development in recent years [8–10]. Up to now, GaN-based ultraviolet PDs have been well developed, including p-i-n photodiodes, Schottky barrier diodes, metal-semiconductor-metal (MSM) photodetectors, and avalanche photodiodes (APDs) [11–14]. Among them, MSM photodetectors are ideal choices for light detection due to the simple fabrication process and suitability for the monolithic integration of an optical receiver [15]. However, at the current stage, a very important target is to improve the photogenerated carrier transport and enhance the photoelectric conversion capability, which is strongly affected by the electric field in the Schottky contact region. The traditional MSM PD separates and transports the photogenerated carriers by utilizing the electric field in the Schottky junctions at two metal/semiconductor interfaces, thereby generating photocurrent. However, the electric field intensity in the Schottky junction is limited by the work function between alloyed metal and the semiconductor. Meanwhile, the screening effect to the electric field by the photogenerated carriers will weaken the electric field, and this can further decrease the carrier transport efficiency [16]. Nevertheless, the aforementioned issues can be partially solved when an asymmetric Schottky barrier structure is used, and by doing so, higher photocurrent and responsivity can be realized [17]. For achieving that goal, an effective method is to fabricate different metal contacts at two ends of the MSM PDs, including utilizing different contact materials and different contact areas, which are known as asymmetric MSM PDs [18,19]. For example, Ref. [17] has demonstrated an asymmetric (Pt–Ag, Pt–Cr) GaN PD that shows the enhanced responsivity. This is attributed to the increased difference in work function between the two contacts, which improves the carrier transport and collection. Moreover, the enhanced carrier transport and collection capability can also be obtained by increasing the electric field magnitude in the absorption layer. It is worth mentioning that using AlGaN/GaN heterostructure can result in a strong electric field in the AlGaN and GaN layers [20]. The strong electric field therein is attributed to the spontaneous polarization and piezoelectric polarization. Most recently, we have fabricated and reported a polarization-assisted GaN-based self-powered MSM PD with AlGaN/GaN heterojunction [21], which enables a large photocurrent and a high responsivity. Nevertheless, the impact of the structural design for polarization-assisted MSM PD on photogenerated carrier transport and photocurrent detectivity has not been discussed until now.

Hence, in this work, we demonstrate an asymmetric GaN-based MSM PD structure, in which an AlGaN polarization layer is inserted between the metal contact on one side and the GaN absorption layer for forming the AlGaN/GaN heterostructure. Our design can utilize the polarization-induced electric field at the AlGaN/GaN interface to imitate the electric field at the metal/semiconductor Schottky contact for the conventional GaN-based MSM PD. Most importantly, we then systematically investigate the optoelectronic performance for the asymmetric MSM PD with different structural designs. Meanwhile, insightful physical mechanisms and discussions are also provided, which reveal that the resulting strong polarization field at the AlGaN/GaN interface can facilitate the transport for the photogenerated carriers. Furthermore, the polarization electric field therein cannot be easily screened by photogenerated carriers, which is helpful to carry large current and avoid current saturation.

2. DEVICE STRUCTURES AND PARAMETERS

By referring to Ref. [20], we design two types of GaN-based PDs in Figs. 1(a) and 1(b). The reference PD (i.e., Device Ref) is shown in Fig. 1(a) with two symmetric Schottky contacts. The schematic device structure for the asymmetric GaN-based MSM PD (i.e., Devices A–F) is shown in Fig. 1(b). The architectural stack for Device Ref and Devices A–F consists of a 4 μm thick unintentionally doped GaN layer ($N_d = 1 \times 10^{16}$ cm^{-3}) for absorbing light. The proposed Devices A–F also have unintentionally doped $Al_yGa_{1-y}N$ layers of different thicknesses ($N_d = 1 \times 10^{16}$ cm^{-3}) as the polarization layer as shown in Fig. 1(b), in which x represents the thickness of the $Al_yGa_{1-y}N$ layer and y represents the Al composition of the $Al_yGa_{1-y}N$ layer. On top of all designed devices, the left anode and the right cathode contacts are considered as Schottky contacts in our calculations, which are both composed of a Ni/Au metal stack for electrodes.

As is shown in Table 1, we stepwisely change the polarization level of the entire device, the Al composition, and the thickness of the $Al_yGa_{1-y}N$ polarization layer for Devices A–F. In order to probe the impact of the different structural parameters on the carrier transport, photocurrent, and responsivity, we conduct the numerical investigations by using the APSYS package [22], which can solve physical equations including current continuity equations, Poisson equations, and drift-diffusion equations self-consistently with proper boundary conditions. When the polarization level is set to 100%, the calculated polarization charge density at the AlGaN/GaN heterojunction is $\sim 3.97 \times 10^{16}$ m^{-2} [21,23]. The work function of Ni is set to 5.15 eV [24]. The absorption coefficient in terms of different wavelengths for GaN material can be referred to Refs. [25,26]. In addition, due to the plasma-related damages during device fabrication, the hole trap level is considered and set to 0.46 eV above the valence band (i.e., $E_V + 0.46$ eV) for all investigated devices except Device Ref, for which the defect density

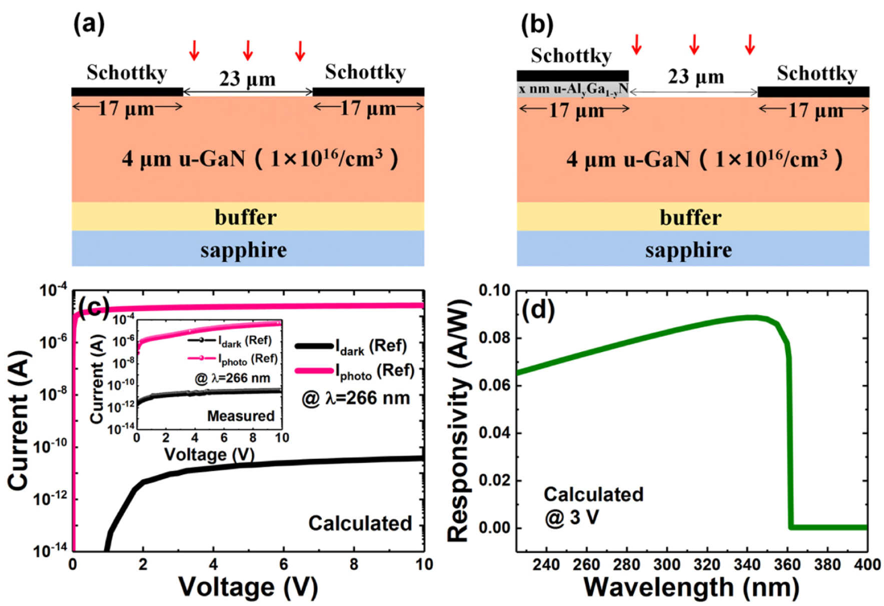

Fig. 1. Schematic cross-sectional structure for (a) Device Ref and (b) the proposed devices. (c) Calculated current-voltage characteristics and (d) calculated spectral response characteristics at 3 V for Device Ref. The inset in figure (c) shows the measured current-voltage characteristics for Device Ref at the applied bias of 3 V. The fabrication process for the experimentally measured devices have been reported in Ref. [21].

Table 1. Structural Information for the Investigated Devices

Device Number	Polarization Level	Thickness of $Al_yGa_{1-y}N$ Layer (x)	Al Composition of $Al_yGa_{1-y}N$ Layer (y)
Device Ref	0%	0 nm	0
Device A1	100%	100 nm	0.10
Device A2	80%	100 nm	0.10
Device A3	60%	100 nm	0.10
Device A4	40%	100 nm	0.10
Device A5	20%	100 nm	0.10
Device A6	10%	100 nm	0.10
Device B1	100%	100 nm	0.15
Device B2	100%	100 nm	0.20
Device B3	100%	100 nm	0.25
Device B4	100%	100 nm	0.30
Device C1	100%	10 nm	0.10
Device C2	100%	50 nm	0.10
Device C3	100%	150 nm	0.10
Device C4	100%	200 nm	0.10
Device D1	100%	10 nm	0.25
Device D2	100%	50 nm	0.25
Device D3	100%	150 nm	0.25
Device D4	100%	200 nm	0.25
Device E1	100%	10 nm	0.30
Device E2	100%	50 nm	0.30
Device E3	100%	150 nm	0.30
Device E4	100%	200 nm	0.30
Device F1	100%	10 nm	0.15
Device F2	100%	10 nm	0.20

is set to 1×10^{19} cm^{-3}, and the capture cross section is set to 2.1×10^{-15} cm^2 [27,28]. The calculated current-voltage characteristics for Device Ref are shown in Fig. 1(c), which shows the same trend as the experimental data in the inset [21]. In addition, we show the calculated spectral response characteristics in Fig. 1(d). We can see that the peak responsivity is around 0.09 A/W at 3 V. The cutoff wavelength is 360 nm, which corresponds to the energy bandgap for the GaN layer. The acceptable agreement validates the models in this work.

3. RESULTS AND DISCUSSION

A. Effectiveness of the Asymmetric GaN-Based MSM PD with an AlGaN Polarization Layer in Improving the Photoelectric Performance

To prove the impact of the $Al_yGa_{1-y}N$ polarization layer on the photoelectric performance improvement, we calculate the dark current and the photogenerated current under the illumination of 266 nm for Devices Ref and A1 in Fig. 2(a). We can get that although the dark current of Device A1 is increased, Device A1 exhibits the enhanced photocurrent simultaneously when compared with Device Ref. Specifically, Device A1 shows the enhanced photocurrent of nearly 1 order of magnitude when compared with Device Ref. This is attributed to the better lateral carrier transport for Device A1. Therefore, we have confirmed that the addition of AlGaN polarization layer is very useful to improve the photoelectric performance for GaN-based MSM PDs. To reveal the self-powered characteristics of Device A1, we calculate and show the spectral response characteristics of Device A1 at 0 V in the inset of Fig. 2(a). The peak responsivity of 0.002 A/W is obtained at the ultraviolet wavelength of 320 nm. The cutoff wavelength is 360 nm, which corresponds to the energy bandgap for the GaN layer. To show the origin of the self-powered photocurrent for Device A1, we also calculate the lateral energy band profiles under the 266 nm illumination for Devices Ref and A1 in Figs. 2(b) and 2(c) at the applied bias of 0 V, respectively. For Device Ref, the Schottky barrier height is the same at both sides so that the lateral energy band profile is symmetrical. Once illuminated with the 266 nm light, the incident photons with an energy larger than or equal to the bandgap of GaN (3.4 eV) can generate electron-hole pairs in the surface of the GaN layer [29]. Then, the same built-in electric field generated from Schottky barriers at both contacts of the Ni/GaN interfaces balances the diffusion of electrons and holes. As a result, the photogenerated current is not able to effectively transport between the two contacts. However, due to the adoption of the polarization AlGaN/GaN heterojunction, the energy band can be aligned as presented in Fig. 2(c), such that the energy barrier heights at the two contacts are strongly unbalanced, which can remarkably promote the transport for the carriers [30]. It is also worth mentioning that the energy band alignment for Device A1 in Fig. 2(c) also favors the carrier transport for the dark current condition, and hence the dark current for Device A1 is also higher than that for Device Ref according to Fig. 2(a).

For better interpretation, Fig. 3(a) shows the lateral electric field profiles for Devices Ref and A1. From Fig. 3(a), we can get that the electric field of Device A1 possesses a wider distribution than that for Device Ref in the range of 17 and 40 μm. Note, such region is not covered by metals and can absorb photons. Therefore, the electric field in the optical absorption region can facilitate the carrier transport. For comparison, the much smaller electric field magnitude in the optical absorption region for Device Ref cannot effectively transport the carriers. We then show the lateral total current profiles for Devices Ref and A1 in Fig. 3(b), which illustrates that the current for Device A1 is much higher than that for Device Ref, especially in the optical absorption region. To eliminate the impact of the electric field on the current level, we then display the electron concentrations and the hole concentrations for Devices Ref and A1 in Figs. 3(c) and 3(d), respectively. We can see that the electrons and holes are more efficiently collected by the left contact for Device A1 when compared with Device Ref. Moreover, the hole concentration at the left contact is much lower than the electron concentration for Device A1, which indicates that the photogenerated current is dominated by electrons for Device A1.

Until now, we have proven that the addition of $Al_yGa_{1-y}N$ polarization layer helps to enhance the photoelectric performance of PD including the photocurrent and the spectral responsivity. We have realized that the electric field in the optical absorption region is essentially important. However, the electric field profiles for the proposed Device A1 can be modified by varying the polarization level, the Al composition of the $Al_yGa_{1-y}N$ layer, the $Al_yGa_{1-y}N$ layer thickness, and so on. Hence, it is essential to investigate the different parameters of the designed PD structures, which are shown in Table 1.

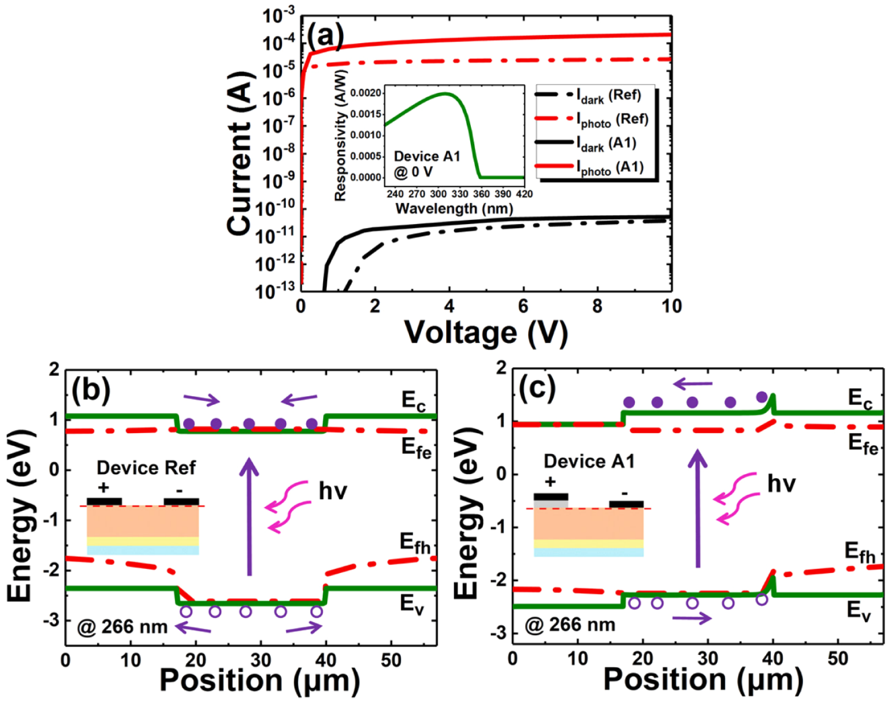

Fig. 2. (a) Dark current and the photogenerated current under the 266 nm illumination in terms of the applied bias for Devices Ref and A1. The inset in figure (a) shows spectral response characteristics for Device A1 at the bias of 0 V. Lateral energy band diagrams of the GaN absorption layer for (b) Device Ref and (c) Device A1 at the equilibrium state of 0 V bias when the illumination light is 266 nm.

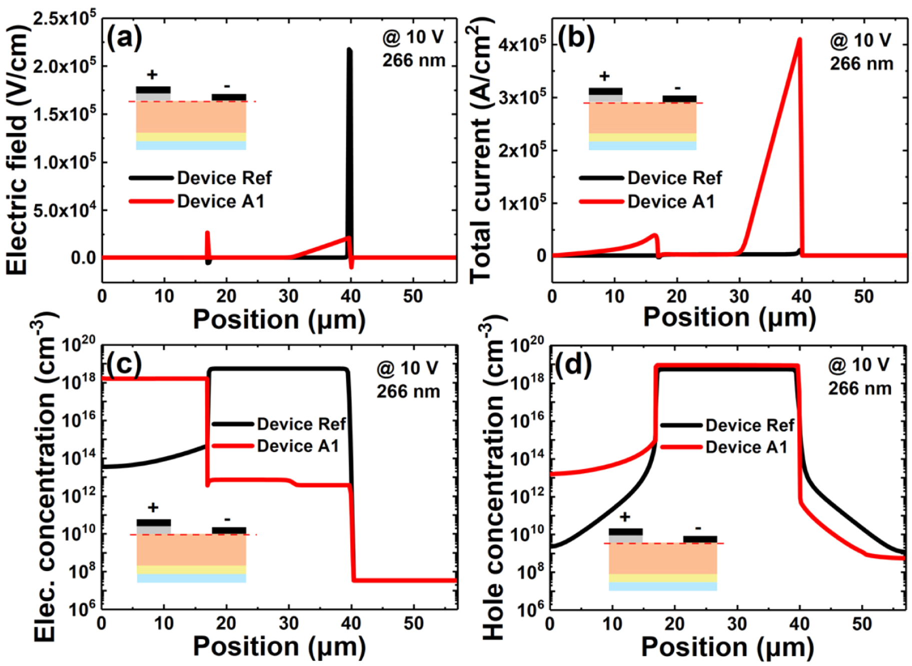

Fig. 3. Profiles of (a) lateral electric field, (b) total current, (c) electron concentration, and (d) hole concentration for Devices Ref and A1 at the applied bias of 10 V when the wavelength of the illumination source is 266 nm.

B. Impact of the Polarization Level on the Photoelectric Performance for the Asymmetric GaN-Based MSM PDs

In order to probe the effect of the polarization level on the photoelectric performance, we compare Devices Ref and A1 to A6. The polarization level ranges from 100% to 10% for Devices A1 to A6, which can be seen in Table 1. In this section, the Al composition and the $Al_yGa_{1-y}N$ layer thickness for Devices A1 to A6 are set to 0.10 and 100 nm, respectively. We firstly show the photocurrent for Devices Ref and A1 to A6 in Fig. 4(a), which presents an increasing trend with the increased polarization level under the same illumination of 266 nm at the applied

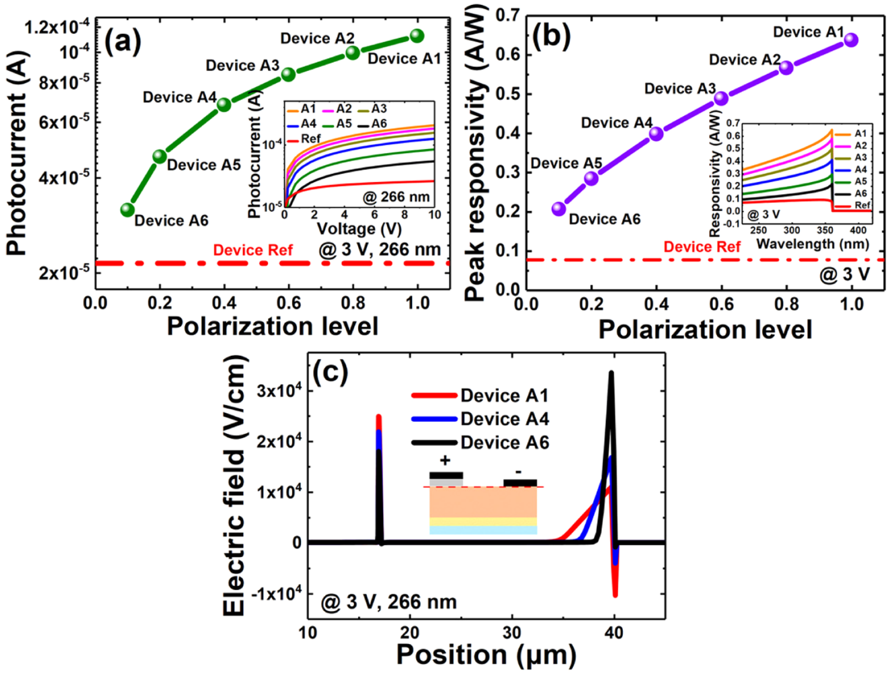

Fig. 4. (a) Photocurrent and (b) peak responsivity for Devices Ref and A1 to A6 at the bias of 3 V. The inset in figure (a) shows photocurrent-voltage characteristics under 266 nm illumination for Devices Ref and A1 to A6. The inset in figure (b) shows spectral response characteristics for Devices Ref and A1 to A6 at the bias of 3 V. (c) Lateral electric field profiles for Devices A1, A4, and A6 at the applied bias of 3 V.

bias of 3 V. Moreover, as shown in Fig. 4(b), the peak responsivity for Devices A1 to A6 also enhances with the increased polarization level at the cutoff response wavelength of 360 nm, which corresponds to the bandgap of GaN approximately [31]. These phenomena confirm that the polarization effect at the GaN/AlGaN heterojunction can enhance the carrier transport at the GaN absorption layer. In addition, the insets of Figs. 4(a) and 4(b) also reveal that the photocurrent and responsivity for Devices A1 to A6 are always higher than that for Device Ref at different voltages and wavelengths, respectively. For the purpose of the demonstration, we further calculate and present the lateral electric field profiles for Devices A1, A4, and A6 in Fig. 4(c) when the bias is 3 V. We can get that the electric field possesses a wider distribution in the range of 17 and 40 μm as the increase of polarization level. This means that a stronger electric field in the light-absorbing region promotes the lateral carrier transport, resulting in higher photocurrent and responsivity.

C. Impact of the Al Composition for the $Al_yGa_{1-y}N$ Polarization Layer on the Photoelectric Performance for the Asymmetric GaN-Based MSM PDs

The Al composition is also an essential parameter for GaN-based MSM PDs with $Al_yGa_{1-y}N$/GaN heterojunction, which can produce different bending levels of the energy band. To get systematic insight into the influence of different Al compositions of the $Al_yGa_{1-y}N$ polarization layer on the photoelectric performance for PDs, we also design Devices B1 to B4 that are shown in Table 1. The polarization level is set to 100%. The Al composition of $Al_yGa_{1-y}N$ layer varies from 0.10 to 0.30 with the alloy step of 0.05.

We first calculate and show the photocurrent and responsivity in terms of the Al composition for Devices A1 and B1 to B4 in Figs. 5(a) and 5(b), respectively. According to Fig. 5(a), the photocurrent decreases as the Al composition increases at the applied bias of 3 V. This is attributed to the increased energy band barrier height, thus suppressing the thermionic emission process for carriers at the GaN/AlGaN interface when the Al composition of $Al_yGa_{1-y}N$ layer increases. The inset in Fig. 5(a) displays the photocurrent-voltage characteristics for the six investigated devices with various Al compositions. We can see that the photocurrent decreases significantly when the Al composition increases to 0.30 (i.e., Device B4) especially at low biases. The photocurrent tends to be close to that of Device Ref when the applied bias gradually increases, which further illustrates that the thermionic emission for carriers can climb over the large energy band barrier height at the GaN/$Al_{0.30}Ga_{0.70}N$ interface only when the applied bias is big enough. Then, the responsivity for the six calculated devices is presented in Fig. 5(b). Excellent agreement is obtained between Figs. 5(a) and 5(b), such that the increased photogenerated current gives rise to the enhanced responsivity when compare Devices A1 and B4. To even better addressing that point, we selectively show the energy band diagrams for Devices A1 and B4 in Figs. 5(c) and 5(d). The conduction band barrier heights (defined as Φ_b) are 104.90 meV and 343.21 meV for Devices A1 and B4, respectively. Thus, we summarize that a properly small Al composition for the AlGaN polarization layer is desired for obtaining the higher photocurrent and the enhanced responsivity.

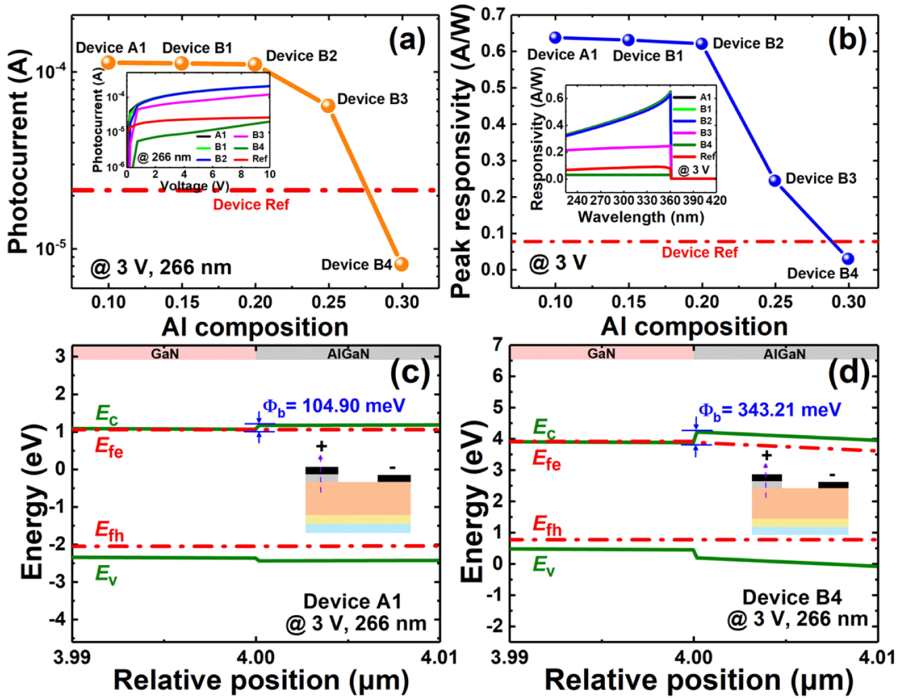

Fig. 5. (a) Photocurrent and (b) peak responsivity for Devices Ref, A1, and B1 to B4 at the bias of 3 V. The insets in figures (a) and (b) show the photocurrent-voltage characteristics under 266 nm illumination and the spectral response characteristics at the applied bias of 3 V for Devices Ref, A1 and B1 to B4, respectively. Energy band diagrams for (c) Device A1 and (d) Device B4 at 3 V when the wavelength of the illumination laser is 266 nm. E_c, E_v, E_{fe}, and E_{fh} represent the conduction band, valence band, quasi-Fermi levels for electrons and holes, respectively.

D. Impact of the $Al_yGa_{1-y}N$ Layer Thickness on the Photoelectric Performance for the Asymmetric GaN-Based MSM PDs

Besides the polarization level and the Al composition for the $Al_yGa_{1-y}N$ layer, the carrier transport can also be affected by the thickness of the $Al_yGa_{1-y}N$ polarization layer, thus influencing the photocurrent and responsivity. In this part, we then design Devices C1 to C4 with various thicknesses of $Al_{0.10}Ga_{0.90}N$ layer (see Table 1). Note, our discussion in Section 3.C indicates that the Al composition of 0.10 for the AlGaN layer can be the optimized values from the point of numerical view. For the purpose of comparison, other Al composition values of 0.25 and 0.30 are also set.

As shown in Fig. 6(a), we investigate the photocurrent as a function of the AlGaN layer thickness by analyzing three groups of devices with different Al composition values. We can clearly find that the photocurrents for the proposed PDs with different thicknesses of $Al_{0.10}Ga_{0.90}N$ layer are all higher than that for Device Ref and the photocurrent hardly depends on the $Al_{0.10}Ga_{0.90}N$ layer thickness. However, as the Al composition increases, the trend shows a gradual decrease. When the $Al_{0.30}Ga_{0.70}N$ layer thickness exceeds 50 nm, the photocurrent value at the applied bias of 3 V is lower than that of Device Ref. Then, we calculate the peak responsivity at the applied bias of 3 V in terms of the AlGaN layer thickness for these devices in Fig. 6(b). Being consistent with the results in Fig. 6(a), the $Al_{0.10}Ga_{0.90}N$ layer thickness has negligible effect on the responsivity. When the Al composition increases to 0.30, the peak responsivity decreases with the increase of AlGaN layer thickness. As has been demonstrated earlier, the thickness of the $Al_{0.10}Ga_{0.90}N$ polarization layer can effectively confine the electric field in the absorption layer. Hence, the variation for the $Al_{0.10}Ga_{0.90}N$ layer thickness does not affect the electric field distribution inside the devices [see Fig. 6(c)]. However, when the Al composition increases, we can see that the electric field of Device E4 is lower than that of Device E1 in the absorption layer according to Fig. 6(d).

E. Impact of the Al Composition of 10 nm thick $Al_yGa_{1-y}N$ Layer on the Photoelectric Performance for the Asymmetric GaN-Based MSM PDs

In this section, the impact of the Al composition for PDs with 10 nm thick $Al_yGa_{1-y}N$ layer on the photoelectric performance is studied. The detailed structural information of the $Al_yGa_{1-y}N$ layer for PDs is summarized in Table 1. Devices C1, D1, E1, F1, and F2 are structurally identical to each other except the Al composition. Meanwhile, Devices A1 and B1 to B4 with various Al compositions for the 100 nm thick $Al_yGa_{1-y}N$ layer are also presented for comparison.

Figures 7(a) and 7(b) show the photocurrent and peak responsivity in terms of different Al compositions of the $Al_yGa_{1-y}N$ layer for Devices Ref, C1, D1, E1, F1, and F2 at the voltage of 3 V. In the meantime, the insets of Figs. 7(a) and 7(b) also demonstrate the photocurrent in terms of the voltage and the responsivity in terms of the wavelength for Devices Ref, C1, D1, E1, F1, and F2. Unlike the observations for Devices A1, B1 to B4, the photocurrent and the responsivity for Devices C1, D1, E1, F1, and F2 are less affected by the Al composition of the

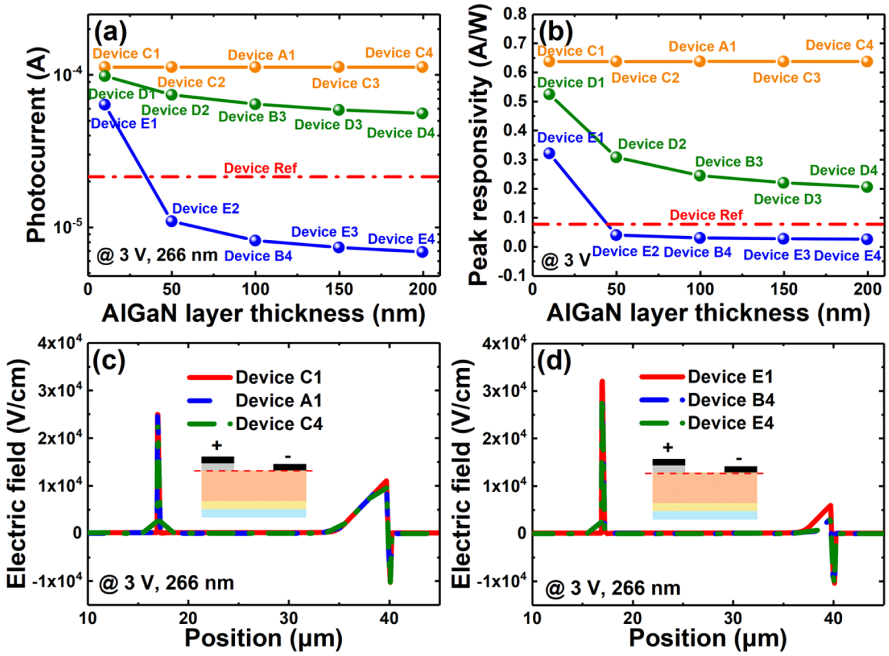

Fig. 6. (a) Photocurrent and (b) peak responsivity for Devices Ref, A1, B3, B4, C1 to C4, D1 to D4 and E1 to E4 at the bias of 3 V. Lateral electric field profiles at 3 V for (c) Devices C1, A1, and C4 and (d) Devices E1, B4, and E4.

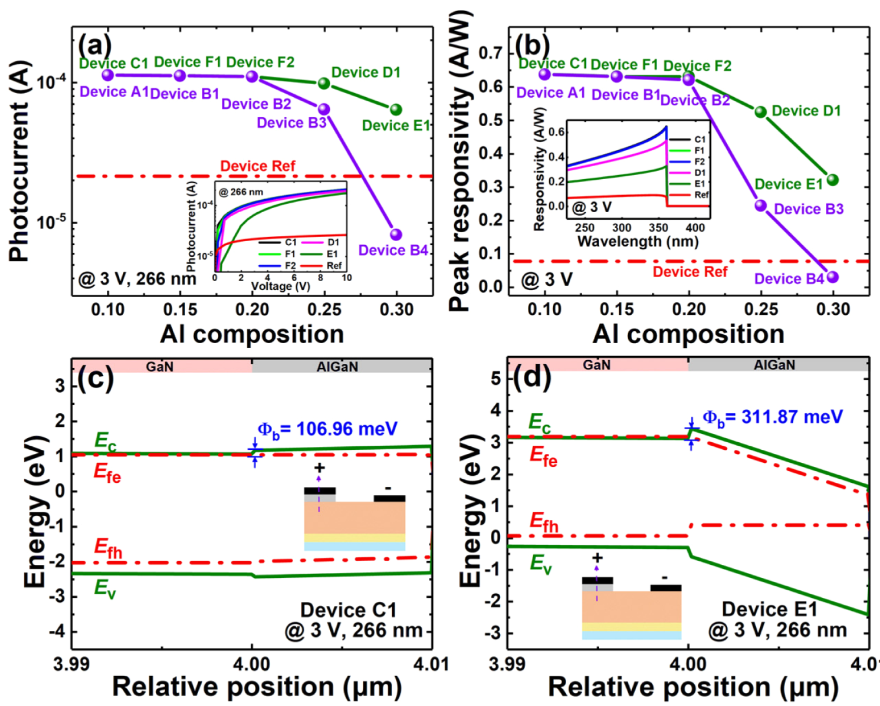

Fig. 7. (a) Photocurrent and (b) peak responsivity at 3 V for Devices Ref, A1, B1 to B4, C1, D1, E1, F1, and F2. The inset in figure (a) shows the photocurrent-voltage characteristics under 266 nm illumination for Devices Ref, C1, D1, E1, F1, and F2. The inset in figure (b) shows the spectral response characteristics at 3 V for Devices Ref, C1, D1, E1, F1, and F2. Energy band diagrams for (c) Device C1 and (d) Device E1 at 3 V when the wavelength of the illumination laser is 266 nm. E_c, E_v, E_{fe}, and E_{fh} represent the conduction band, valence band, quasi-Fermi levels for electrons and holes, respectively.

$Al_yGa_{1-y}N$ polarization layer. However, the values of the photocurrent and the responsivity for these five devices still decrease with the increase of Al composition for the thin $Al_yGa_{1-y}N$ layer. As shown in Figs. 7(c) and 7(d), this is mainly because that the energy band barrier height at the GaN/$Al_yGa_{1-y}N$ interface becomes higher when the Al composition of $Al_yGa_{1-y}N$ polarization layer increases, e.g., the conduction band barrier heights (defined as Φ_b) are 106.96 meV and 311.87 meV for

Devices C1 and E1, respectively. Therefore, the carriers are difficult to climb over the GaN/$Al_yGa_{1-y}N$ barrier height when the Al composition increases to 0.30. Thus, the larger photocurrent and the enhanced responsivity are obtained for Device C1 when compared with Device E1 according to Figs. 7(a) and 7(b), respectively. Note, if we further analyze Devices A1, B4, C1 and E1, we also find that the energy band barrier heights for electrons have obvious changes [see Figs. 5(c), 5(d), 7(c), and 7(d)]. Devices A1 and C1 have the similar conduction band barrier heights, and therefore two devices show the similar photocurrent and responsivity. For Devices B4 and E1, the conduction band barrier height is reduced by 31.34 meV when the $Al_{0.30}Ga_{0.70}N$ layer is thinned from 100 to 10 nm. Therefore, the carrier transport can be favored for Device E1, thus increasing the photocurrent and the responsivity. In general, the use of a thin polarization layer is a practicable method to get the better photoelectric performance, especially for high Al composition $Al_yGa_{1-y}N$ layer.

4. CONCLUSION

To summarize, we have numerically analyzed and demonstrated that the asymmetric GaN-based MSM photodetector with $Al_yGa_{1-y}N$ polarization layer in enhancing the photocurrent and the responsivity. The essence is that the polarization induced electric field in the absorption layer can promote the carrier transport, which favors the increased photocurrent and enhanced responsivity for the proposed PD structures. Moreover, the impact of the polarization level, Al composition, and $Al_yGa_{1-y}N$ polarization layer thickness on the photoelectric performance is also investigated for the proposed PDs. We prove that the higher polarization level is required so that the even stronger electric field in the absorption layer can be obtained, thus improving the carrier transport capability. However, we also find that the $Al_yGa_{1-y}N$ polarization layer shall be properly thin so that the carrier transport will not be sacrificed at the GaN/$Al_yGa_{1-y}N$ interface when the Al composition of the $Al_yGa_{1-y}N$ layer increases. We believe that the structure design and physical mechanism analysis reported here in this work are very important for researchers to optimize GaN-based MSM PDs at lower cost.

Funding. National Natural Science Foundation of China (62074050); State Key Laboratory of Reliability and Intelligence of Electrical Equipment, Hebei University of Technology (EERI_PI2020008); Jiangsu Provincial Key Laboratory of Photonic and Electronic Materials Sciences and Technology, Nanjing University (njuzds2021-005).

Disclosures. The authors declare no conflicts of interest.

Data Availability. Data underlying the results presented in this paper are not publicly available at this time but may be obtained from the authors upon reasonable request.

REFERENCES

1. M. Khaouani, A. Hamdoune, H. Bencherif, Z. Kourdi, and L. Dehimi, "An ultra-sensitive AlGaN/AlN/GaN/AlGaN photodetector: proposal and investigation," Optik **217**, 164797 (2020).
2. D. Zhang, C. Chu, K. Tian, J. Kou, W. Bi, Y. Zhang, and Z.-H. Zhang, "Improving hole injection from p-EBL down to the end of active region by simply playing with polarization effect for AlGaN based DUV light-emitting diodes," AIP Adv. **10**, 065032 (2020).
3. M. Xiao, Y. Ma, K. Liu, K. Cheng, and Y. Zhang, "10 kV, 39 mΩ·cm^2 multi-channel AlGaN/GaN Schottky barrier diodes," IEEE Electron Device Lett. **42**, 808–811 (2021).
4. H. Zhang, F. Liang, K. Song, C. Xing, D. Wang, H. Yu, C. Huang, Y. Sun, L. Yang, X. Zhao, H. Sun, and S. Long, "Demonstration of AlGaN/GaN-based ultraviolet phototransistor with a record high responsivity over 3.6 $\times$ 10^7 A/W," Appl. Phys. Lett. **118**, 242105 (2021).
5. E. Muñoz, "(Al,In,Ga)N-based photodetectors. Some materials issues," Phys. Status Solidi B **244**, 2859–2877 (2007).
6. E. Monroy, F. Omnés, and F. Calle, "Wide-bandgap semiconductor ultraviolet photodetectors," Semicond. Sci. Technol. **18**, R33–R51 (2003).
7. M. A. Khan, J. N. Kuznia, D. T. Olson, J. M. Van Hove, M. Blasingame, and L. F. Reitz, "High-responsivity photoconductive ultraviolet sensors based on insulating single-crystal GaN epilayers," Appl. Phys. Lett. **60**, 2917–2919 (1992).
8. D. Wang, C. Huang, X. Liu, H. Zhang, H. Yu, S. Fang, B. S. Ooi, Z. Mi, J. He, and H. Sun, "Highly uniform, self-assembled AlGaN nanowires for self-powered solar-blind photodetector with fast-response speed and high responsivity," Adv. Opt. Mater. **9**, 2000893 (2020).
9. S. Fang, D. Wang, X. Wang, X. Liu, Y. Kang, H. Yu, H. Zhang, W. Hu, J. He, H. Sun, and S. Long, "Tuning the charge transfer dynamics of the nanostructured GaN photoelectrodes for efficient photoelectrochemical detection in the ultraviolet band," Adv. Funct. Mater. **31**, 2103007 (2021).
10. D. Wang, X. Liu, S. Fang, C. Huang, Y. Kang, H. Yu, Z. Liu, H. Zhang, R. Long, Y. Xiong, Y. Lin, Y. Yue, B. Ge, T. K. Ng, B. S. Ooi, Z. Mi, J.-H. He, and H. Sun, "Pt/AlGaN nanoarchitecture: toward high responsivity, self-powered ultraviolet-sensitive photodetection," Nano Lett. **21**, 120–129 (2021).
11. X. Bao, J. Xu, C. Li, H. Qiao, Y. Zhang, and X. Li, "Temperature and frequency dependence of negative differential capacitance in a planar GaN-based p-i-n photodetector," J. Alloy. Compd. **581**, 289–292 (2013).
12. N. Zainal, M. A. Ahmad, W. Maryam, M. E. A. Samsudin, S. N. Waheeda, M. I. M. Taib, and Z. Hassan, "Performance of polycrystalline GaN based metal-semiconductor-metal (MSM) photodetector with different contact," Superlattices Microstruct. **138**, 106369 (2020).
13. F. Bouzid, L. Dehimi, and F. Pezzimenti, "Performance analysis of a Pt/n-GaN schottky barrier UV detector," J. Electron. Mater. **46**, 6563–6570 (2017).
14. J. Zheng, L. Wang, X. Wu, Z. Hao, C. Sun, B. Xiong, Y. Luo, Y. Han, J. Wang, H. Li, M. Li, J. Kang, and Q. Li, "The influence of structure parameter on GaN/AlN periodically stacked structure avalanche photodiode," IEEE Photon. Technol. Lett. **29**, 2187–2190 (2017).
15. T. Li, L. Long, Z. Hu, R. Wan, X. Gong, L. Zhang, Y. Yuan, J. Yan, W. Zhu, L. Wang, and J. Li, "Three-dimensional metal–semiconductor–metal AlN deep-ultraviolet detector," Opt. Lett. **45**, 3325–3328 (2020).
16. K. Shimomura, "Proposal of field-effect-type photodetector using field-screening effect in the absorption of light," Jpn. J. Appl. Phys. **31**, L1757–L1759 (1992).
17. D. Li, X. Sun, H. Song, Z. Li, H. Jiang, Y. Chen, G. Miao, and B. Shen, "Effect of asymmetric schottky barrier on GaN-based metal-semiconductor-metal ultraviolet detector," Appl. Phys. Lett. **99**, 261102 (2011).
18. S. K. Jain, N. Aggarwal, S. Krishna, R. Kumar, S. Husale, V. Gupta, and G. Gupta, "GaN-UV photodetector integrated with asymmetric metal semiconductor metal structure for enhanced responsivity," J. Mater. Sci. Mater. Electron. **29**, 8958–8963 (2018).
19. L. Dong, J. Yu, R. Jia, J. Hu, Y. Zhang, and J. Sun, "Self-powered MSM deep-ultraviolet β-Ga_2O_3 photodetector realized by an asymmetrical pair of Schottky contacts," Opt. Mater. Express **9**, 1191–1199 (2019).
20. I. P. Smorchkova, C. R. Elsass, J. P. Ibbetson, R. Vetury, B. Heying, P. Fini, E. Haus, S. P. DenBaars, J. S. Speck, and U. K. Mishra, "Polarization-induced charge and electron mobility in AlGaN/GaN heterostructures grown by plasma-assisted molecular-beam epitaxy," J. Appl. Phys. **86**, 4520–4526 (1999).

21. J. Wang, C. Chu, K. Tian, J. Che, H. Shao, Y. Zhang, K. Jiang, Z.-H. Zhang, X. Sun, and D. Li, “Polarization assisted self-powered GaN-based UV photodetector with high responsivity,” Photon. Res. **9**, 734–740 (2021).
22. Crosslight software inc., “APSYS 2018 and APSYS technical manuals,” [Online]. Available: http://www.crosslight.com.
23. M. Brendel, M. Helbling, A. Knigge, F. Brunner, and M. Weyers, “Measurement and simulation of top- and bottom-illuminated solar-blind AlGaN metal-semiconductor-metal photodetectors with high external quantum efficiencies,” J. Appl. Phys. **118**, 244504 (2015).
24. A. Motayed, A. V. Davydov, M. D. Vaudin, I. Levin, J. Melngailis, and S. N. Mohammad, “Fabrication of GaN-based nanoscale device structures utilizing focused ion beam induced Pt deposition,” J. Appl. Phys. **100**, 024306 (2006).
25. J. F. Muth, J. D. Brown, M. A. L. Johnson, Z. Yu, R. M. Kolbas, J. W. Cook, and J. F. Schetzina, “Absorption coefficient and refractive index of GaN, AlN and AlGaN alloys,” MRS Internet J. Nitride Semicond. Res. **4**, 502–507 (1999).
26. M. Brendel, M. Helbling, A. Knauer, S. Einfeldt, A. Knigge, and M. Weyers, “Top- and bottom-illumination of solar-blind AlGaN metal-semiconductor-metal photodetectors,” Phys. Status Solidi A **212**, 1021–1028 (2015).
27. W. Götz, N. M. Johnson, D. P. Bour, M. D. McCluskey, and E. E. Haller, “Local vibrational modes of the Mg–H acceptor complex in GaN,” Appl. Phys. Lett. **69**, 3725–3727 (1996).
28. T. Narita, Y. Tokuda, T. Kogiso, K. Tomita, and T. Kachi, “The trap states in lightly Mg-doped GaN grown by MOVPE on a freestanding GaN substrate,” J. Appl. Phys. **123**, 161405 (2018).
29. A. Gundimeda, S. Krishna, N. Aggarwal, A. Sharma, N. D. Sharma, K. K. Maurya, S. Husale, and G. Gupta, “Fabrication of non-polar GaN based highly responsive and fast UV photodetector,” Appl. Phys. Lett. **110**, 103507 (2017).
30. Z.-H. Zhang, L. Li, Y. Zhang, F. Xu, Q. Shi, B. Shen, and W. Bi, “On the electric-field reservoir for III-nitride based deep ultraviolet light-emitting diodes,” Opt. Express **25**, 16550–16559 (2017).
31. A. Chatterjee, S. K. Khamari, R. Kumar, S. Porwal, A. Bose, and T. K. Sharma, “Role of threading dislocations and point defects in the performance of GaN-based metal-semiconductor-metal ultraviolet photodetectors,” Superlattices Microstruct. **148**, 106733 (2020).

202.194.19.103 {ts '2022-06-08 00:08:46'}